Spin–Orbit Couplings for Nonadiabatic Molecular Dynamics at the ΔSCF Level

Mališ, Momir ; Vandaele, Eva ; Luber, Sandra

DOI: https://doi.org/10.1021/acs.jctc.1c01046

Spin-Orbit Couplings for Nonadiabatic Molecular Dynamics at the $\triangle$SCF Level

Momir Mališ,* Eva Vandaele, and Sandra Luber*

Department of Chemistry, University of Zürich, Winterthurerstrasse 190, 8057 Zürich, Switzerland

E-mail: momir.malis@uzh.ch; sandra.luber@chem.uzh.ch

Abstract

A procedure for the calculation of spin-orbit coupling (SOC) at the delta self-consistent field (ΔSCF) level of theory is presented. Singlet and triplet excited electronic states obtained with the ΔSCF method are expanded into a linear combination of singly-excited Slater determinants composed of ground electronic state Kohn–Sham orbitals. This alleviates the nonorthogonality between excited and ground electronic states and introduces a framework, similar to the auxiliary wave function at the time-dependent density functional theory (TD-DFT) level, for the calculation of observables. The ΔSCF observables of the formaldehyde system were compared to reference TD-DFT values. Our procedure gives all components (energies, gradients, nonadiabatic couplings, and SOC terms) at the ΔSCF level of theory for conducting efficient, full-atomistic nonadiabatic molecular dynamics with intersystem crossing, particularly in condensed phase systems.

1 Introduction

Only by including states of different multiplicities a complete picture of nonadiabatic (NA) phenomena initiated by light absorption can usually be obtained. Even though almost all life building block molecules are closed-shell electronic systems and their singlet electronic states are directly involved in photoabsorption and nonradiative deactivation through conical intersections, a number of recent works have shown that triplet electronic states play a nonnegligible role in the photodynamics of these systems, and contribute to their photostability.[1–7] The efficiency of modern organic light-emitting diode-based displays,[8–13] as well as novel phototherapeutic pharmaceuticals[14–18] are just a few recent technological innovations relying on harvesting the triplet excited electronic states. Thus the ability to simulate the singlet-triplet interaction processes is at the very core of understanding NA phenomena.

The delta self-consistent field (ΔSCF) method is an extension of density functional theory (DFT) concepts for the description of any stationary excited electronic state.[19–28] As a variational method, unlike its perturbative time-dependent (TD) DFT counterpart, the ΔSCF method optimizes a guess electronic density which approximates an excited electronic state. However, the low computational cost of the ground state energy calculation and the ability to selectively model excited electronic states of interest in a dense manifold of various electronic excitations make the ΔSCF method attractive for simulating NA mechanisms in condensed phase systems.[28–33] Because the ΔSCF method just optimizes a guess electron density, it has to be provided, either by an educated guess or, for instance, TD-DFT can provide the initial guess excited electronic state density,[31,32] whereas a number of optimization procedures can be chosen for its successful convergence.[22,24–26,31,34–40] In ΔSCF NA-MD, a converged density from a previous step can be used for the guess electron density in the next step. As the method is ignorant to the presence of other electronic states, it is advised to check the ordering and characters of electronic states along the ΔSCF trajectory with another electronic structure method which can directly generate a set of electronic states, for example with TD-DFT, especially when conducting the NA-MD for the first time. For

best practice, a set of preliminary NA-MD trajectories obtained with ΔSCF can be recalculated and compared with a possibly more accurate (wave function based) electronic structure method over a wider range of configuration space which validates the applicability of ΔSCF for the chosen system and also for selection of excited electronic states for the manifold of active excited electronic states in NA-MD. While the construction of an excited electronic state of particular multiplicity, most notably the singlet and triplet excited electronic states, is achieved by the proper occupation of alpha and beta spin electronic densities,[41,42] in a number of cases these details were overlooked, or the states were not of precise multiplicity due to the unrestricted construction of the alpha and beta spin electronic densities.[25,35,36] However, to our best knowledge, no attempt to model the singlet–triplet interaction has been conducted at this level of theory, motivating us to examine the inclusion of the singlet-triplet interaction, starting with the one-electron spin-orbit coupling (SOC) at the ΔSCF level. The one-electron SOC terms are generally the strongest contributions of a far more complex Breit–Pauli Hamiltonian,[43,44] and although in light-atom systems they might compete with two-electron contributions,[45] for the demonstration purpose we just focus on the one-electron SOC term.

As the ΔSCF method separately optimizes each excited electronic state, constructing SOC terms or other observables which couple pairs of distinct excited electronic states becomes problematic due to the nonorthogonality between different excited electronic states, since different sets of molecular orbitals (MOs) are used for each electronic state which are not mutually orthogonal, hereby introducing nonphysical properties. In the case of obtaining transition dipole moments necessary for the estimation of absorption properties, Bourne Worster and collaborators have used symmetric orthogonalization to transform the original transition density matrix into its orthogonalized counterpart.[46] Pradhan *et al.* have used the Löwdin transformation technique[47] to retransform the entire TD Schrödinger equation constructed from nonorthogonal wave functions to its hermitian form to preserve the total energy and the total population of all included electronic states.[25] Their wave functions

are single Slater determinants that directly approximate the wave functions associated with each electronic state density, even though the latter, when made of fractional occupation numbers, cannot be derived from a single determinant. Thus, in order to have a mapping between excited electron density and a single Slater determinant, the procedure is limited to excited electronic states with a dominant single reference character. In other words, such excited electronic states can be described by a single Slater determinant composed of the Kohn–Sham (KS) orbitals, where the square of the determinant gives the corresponding excited electronic state density.

The excited electronic state Slater determinant is not orthogonal to any other electronic state but can be expanded into a linear combination of Slater determinants composed of KS orbitals of another electronic state, for example, the ground electronic state. Such configuration interaction (CI) representation of a singly-excited Slater determinant is complete in the limit of full CI and an infinite basis set and can be made fully orthogonal to the electronic state used for its expansion.[48] By truncating such expansion to the superposition of singly-excited Slater determinants (CIS equivalent) we (i) show that it is mathematically similar to the auxiliary wave function used for determining observables within linear-response (LR) TD-DFT,[49,50] and (ii) use them to determine the SOC terms and other observables.

We calculated the one-electron SOC and transition dipole moment terms for the isolated formaldehyde system which was previously used for LR-TD-DFT SOC benchmarking.[50,51] The photodynamics of electronically excited formaldehyde has been extensively studied, displaying several deactivation channels from its first singlet excited electronic state (S1), each characterized by a corresponding barrier height.[52] All deactivation channels compete with fluorescence and, depending on the exact vibronic excitation, the S1 state has a lifetime of a few to few tens of nanoseconds.[53] The first triplet excited electronic state (T1) also plays a key role in the homolytic C–H bond dissociation of the radical channel.[54] Bowman and coauthors simulated these mechanisms with NA molecular dynamics (MD) simulations employing global potential energy surfaces constructed for the electronic ground, S1, and T1

states on a timescale of several hundred picoseconds.[55–57] Such timescales are impractical for ΔSCF NA-MD simulations, but even a fraction of the full NA-MD represents an unbiased validation of the one-electron SOC terms over a wider configuration space range. In addition, SOC terms between few lowest singlet and triplet excited electronic states were determined for thioformaldehyde, cyclopropanone, uracil, *p*-nitrophenol, and triazatriangulenium cation (further designated as TATA+) at single point geometries and compared with LR-TD-DFT countervalues.

The paper is structured as follows: Section 2 gives a detailed derivation of the one-electron SOC terms at the ΔSCF level and the CIS expansion of the single reference excited electronic state density; Section 3 explains the implementation and the setup used for evaluating the SOC terms; which are presented in Section 4; followed by the overall conclusions in Section 5.

2 Theory

2.1 ΔSCF formulation of SOC terms

In this paper the SOC is approximately described by the nuclear–electron magnetic interaction term of the Breit–Pauli Hamiltonian[43,44]

$$\hat{H}_{\mathrm{SOC}} = \frac{\mu_0 e^2 g_e}{8\pi m_e^2} \sum_{i=1}^{N_e} \sum_{n=1}^{N_n} \frac{Z_n^*}{|\boldsymbol{r}_{in}|^3} \left(\hat{\boldsymbol{r}}_{in} \times \hat{\boldsymbol{p}}_i\right) \cdot \hat{\boldsymbol{s}}_i, \tag{1}$$

between all N_e electrons and N_n nuclei of the system. Two electron contributions to the SOC are neglected. The $\boldsymbol{r}_{in}$ designates the distance vector between n-th nucleus and electron i, whose momentum and spin operators are given by $\hat{\boldsymbol{p}}_i$ and $\hat{\boldsymbol{s}}_i$, respectively. Bold symbols designate three-dimensional Cartesian vectors in a coordinate system with an arbitrary origin. The Z_n^* designates the n-th nucleus effective nuclear charge, while m_e, e, and g_e are the electron's rest mass, charge, and g-factor, respectively, μ_0 is the vacuum permeability. Taking the position representation of the i-th electron momentum operator ($\imath\hbar\boldsymbol{\nabla}_i$) and the

Pauli matrices for the three components of the spin operator ($\hat{s}_{ij} = (\hbar/2)\hat{\sigma}_{ij}$, $j = x, y, z$) together with an approximate value 2 for the electron g-factor, the above expression takes the form

$$\hat{H}_{\mathrm{SOC}} = \imath \frac{\alpha^2}{2} E_h a_0^3 \sum_{j=x,y,z} \sum_{i=1}^{N_e} \hat{\xi}_{ij} \hat{\sigma}_{ij}, \tag{2}$$

where the nuclear terms are assembled into an orbital angular momentum operator for every electron

$$\hat{\xi}_{ij} = \left\{ \sum_{n=1}^{N_n} \frac{Z_n^*}{|\boldsymbol{r}_{in}|^3} \left(\hat{\boldsymbol{r}}_{in} \times \boldsymbol{\nabla}_i \right) \right\}_j . \tag{3}$$

The constants rearrange into the fine structure constant ($\alpha = \mu_0 e^2 c/(4\pi\hbar)$), and definitions of Hartree ($E_h = m_e c^2 \alpha^2$) and Bohr radius ($a_0 = \hbar/(m_e c\alpha)$). Atomic units are used from this point onward. The operator $\hat{\xi}$ is antisymmetric along all j components so that the expression (2) is hermitian.

Within ΔSCF, the excited electronic state energy is obtained variationally from DFT by optimizing the electronic density for each spin channel, i.e., α electrons' density ($\rho_\alpha^i(\boldsymbol{r})$) and β electrons' density ($\rho_\beta^i(\boldsymbol{r})$), so that their final values approximate the corresponding electronic density of a stationary excited electronic state i. The electronic densities are constructed from KS orbitals ($\varphi_{j\varsigma}$) associated to each spin channel $\varsigma \in \{\alpha, \beta\}$ as

$$\rho_\varsigma^i(\boldsymbol{r}) = \sum_j n_{j\varsigma}^i \left| \varphi_{j\varsigma}^i(\boldsymbol{r}) \right|^2 , \tag{4}$$

where the sum of the orbital occupation numbers $n_{j\varsigma}^i$ equals to the total number of electrons in the system ($\sum_{j\varsigma} n_{j\varsigma} = N_e$), and the KS orbitals are one-particle eigenfunctions of the KS equation

$$\left\{ -\frac{1}{2}\nabla^2 + w(\boldsymbol{r}) + \int \frac{\rho_\alpha^i(\boldsymbol{r}') + \rho_\beta^i(\boldsymbol{r}')}{|\boldsymbol{r} - \boldsymbol{r}'|} \, d\boldsymbol{r}' + v_{\mathrm{xc}}^\varsigma[\rho_\alpha^i, \rho_\beta^i](\boldsymbol{r}) \right\} \varphi_{j\varsigma}^i(\boldsymbol{r}) = \epsilon_{j\varsigma}^i \varphi_{j\varsigma}^i(\boldsymbol{r}). \tag{5}$$

Terms in the curly brackets on the left-hand side are, from left to right, the kinetic energy, the external potential, the Coulomb potential, and the exchange–correlation (xc) potential,

where the latter two are functionals of the electronic density. The difference between the xc potentials associated with each spin channel (note the spin state index of the xc potential) reflects on the difference between the two electronic spin densities and vice versa.[58] Due to this the KS equations (5) together with (4) are solved self-consistently so that they minimize the i-th electronic state energy

$$E^i = \int \Bigg(-\frac{1}{2}\sum_{j,\varsigma} n^i_{j\varsigma}\varphi^i_{j\varsigma}(\boldsymbol{r})\nabla^2\varphi^i_{j\varsigma}(\boldsymbol{r}) + v^{\alpha}_{\mathrm{xc}}[\rho^i_{\alpha},\rho^i_{\beta}](\boldsymbol{r})\rho^i_{\alpha}(\boldsymbol{r}) + v^{\beta}_{\mathrm{xc}}[\rho^i_{\alpha},\rho^i_{\beta}](\boldsymbol{r})\rho^i_{\beta}(\boldsymbol{r}) + \left\{ w(\boldsymbol{r}) + \frac{1}{2}\int \frac{\rho^i_{\alpha}(\boldsymbol{r}') + \rho^i_{\beta}(\boldsymbol{r}')}{|\boldsymbol{r}-\boldsymbol{r}'|}\, d\boldsymbol{r}' \right\} \big(\rho^i_{\alpha}(\boldsymbol{r}) + \rho^i_{\beta}(\boldsymbol{r})\big) \Bigg) d\boldsymbol{r}, \tag{6}$$

while simultaneously assuring that electronic densities resemble those of an excited state with defined spin multiplicity by appropriately keeping adequate occupation numbers associated with the selected KS-MOs through equation (4). The latter can be achieved, e.g., by applying the Initial Maximum Overlap Method.[36,59]

For closed-shell systems, which have an even number of electrons, the two lowest energy excited state multiplicities are in general the singlet (S) and triplet (T) electronic states, the latter being triply degenerate, whose degenerate states differ in the projection of the total spin. In the wave function formulation, these states are eigenfunctions of the total and projection spin operators, but within DFT, the singlet and the triplet state with spin projection $S_{tot.,z} = 0$ cannot be distinguished based on their corresponding spin densities.[60] As a consequence, the DFT exchange–correlation functional, which is based only on the electronic spin densities, cannot associate the correct energy to the $S_{tot.,z} = 0$ triplet state. For ΔSCF at a DFT level certain requirements have to be imposed to construct the proper electronic densities from which SOC terms can be determined. If the excited electronic state is of a single reference character, then that excited state can be approximated with a single Slater determinant in which one occupied (o) spin KS-MO is replaced by a virtual (v) spin KS-MO. The set of occupied and virtual KS-MOs for each excited electronic state resembles by orbitals' spatial shape and character the MOs of the ground electronic state, but are not orthogonal to

it nor to any other electronic state set of KS-MOs. Several singly-excited determinants might need to be combined to match the excited electronic state's multiplicity. Unlike the Hartree–Fock orbitals, KS orbitals are by their definition not intended to reproduce the system's wave function but its electron density, and are considered here only as means to calculate SOC terms and other observables. There is no formal proof for this approach but it is mathematically similar to the typically used auxiliary wave functions approach for the determination of observables within the TD-DFT framework,[49,61–64] including SOC.[50,51,65,66] It should be noted that the auxiliary wave functions hold only for the Tamm–Dancoff approximation[49,67] of LR-TD-DFT when compared to more accurate equation-of-motion formulation.[68]

The approximate wave function for the ground electronic state $|\psi^{\mathrm{S0}}\rangle$ is

$$|\psi^{\mathrm{S0}}\rangle \approx |\phi^{\mathrm{S0}}\rangle = \frac{1}{\sqrt{N_e!}} \det\left(\varphi^{\mathrm{S0}}_{1\alpha}\boldsymbol{\alpha}, \varphi^{\mathrm{S0}}_{1\beta}\boldsymbol{\beta}, \ldots, \varphi^{\mathrm{S0}}_{o\alpha}\boldsymbol{\alpha}, \varphi^{\mathrm{S0}}_{o\beta}\boldsymbol{\beta}, \ldots, \varphi^{\mathrm{S0}}_{\frac{N_e}{2}\alpha}\boldsymbol{\alpha}, \varphi^{\mathrm{S0}}_{\frac{N_e}{2}\beta}\boldsymbol{\beta}\right). \qquad (7)$$

The det on the right-hand side is a shorthand for the Slater determinant composed of all the listed occupied KS orbitals over all N_e electron coordinates, while bold symbols $\boldsymbol{\alpha}$ and $\boldsymbol{\beta}$ indicate individual electron spin state functions. We keep the designation $|\psi\rangle$ for electronic wave functions that we approximate with Slater determinants indicated with symbol $|\phi\rangle$. Here we adopt a convention of indicating the electronic state by index in the upper-right superscript, that on the right-hand side of expressions indicates to which electronic state the corresponding set of KS-MOs belong. The square of such wave function integrated over all but one electron index and spin state yields the ground state electron density expression (4) with occupation numbers equal to one for all occupied KS orbitals and zero for virtual ones. The use of a restricted-open (RO) KS formulation assures that the spatial KS orbitals are identical for both spin states ($\varphi_{j\alpha} = \varphi_{j\beta}$, written from now as φ_j) and guarantees a singlet

electronic state. Similarly, an i-th singlet excited state Si of an $o \rightarrow v$ transition character is

$$
\begin{aligned}
|\psi^{\mathrm{S}i}\rangle &\approx \frac{1}{\sqrt{2}}\big(|\phi^{\mathrm{S}i}_{o\alpha\rightarrow v\alpha}\rangle + |\phi^{\mathrm{S}i}_{o\beta\rightarrow v\beta}\rangle \big) \\
&= \frac{1}{\sqrt{2N_e!}}\Big\{ \det\Big(\varphi^{\mathrm{S}i}_1\boldsymbol{\alpha}, \varphi^{\mathrm{S}i}_1\boldsymbol{\beta}, \ldots, \underline{\varphi^{\mathrm{S}i}_v\boldsymbol{\alpha}}, \varphi^{\mathrm{S}i}_o\boldsymbol{\beta}, \ldots, \varphi^{\mathrm{S}i}_{\frac{N_e}{2}}\boldsymbol{\alpha}, \varphi^{\mathrm{S}i}_{\frac{N_e}{2}}\boldsymbol{\beta}\Big) + \\
&\qquad \det\Big(\varphi^{\mathrm{S}i}_1\boldsymbol{\alpha}, \varphi^{\mathrm{S}i}_1\boldsymbol{\beta}, \ldots, \varphi^{\mathrm{S}i}_o\boldsymbol{\alpha}, \underline{\varphi^{\mathrm{S}i}_v\boldsymbol{\beta}}, \ldots, \varphi^{\mathrm{S}i}_{\frac{N_e}{2}}\boldsymbol{\alpha}, \varphi^{\mathrm{S}i}_{\frac{N_e}{2}}\boldsymbol{\beta}\Big) \Big\}.
\end{aligned} \tag{8}
$$

The subscript $o\varsigma \rightarrow v\sigma$ generally designates which occupied (o) KS-MO and its spin function (ς) are replaced in the Slater determinant with a virtual (v) KS-MO and its new spin function (σ) when compared to the ground electronic state Slater determinant (7). In the above electronic state changed MOs are highlighted by underlines on the right-hand side. It should be noted that the usual designations occupied (o) and virtual (v) KS-MOs are only for the relation of excited electronic state MOs to the ground electronic state MOs. This serves the purpose of designating the electronic transition type in terms of ground electronic state MOs even though the indicated v (spin-)KS-MO is (half-)occupied for the excited electronic states. The corresponding electron density for each spin channel of such singlet state is $\rho^{\mathrm{S}i}_{\varsigma} = |\varphi^{\mathrm{S}i}_1|^2 + \ldots + (1/2)|\varphi^{\mathrm{S}i}_o|^2 + (1/2)|\varphi^{\mathrm{S}i}_v|^2 + \ldots + |\varphi^{\mathrm{S}i}_{\frac{N_e}{2}}|^2$, showing half-occupations of the o and v KS orbitals. In terms of the total electron density, $\rho_\alpha + \rho_\beta$, their occupation is exactly one as in the case of restricted KS orbital ΔSCF.[31,34,38,69,70] By fixing and rounding the occupation numbers to values 0, 1/2 and 1 in the RO-KS SCF optimization, one assures that the converged density can be represented with the Slater determinant (8). Similarly, the three degenerate triplet states are

$$
|\psi^{\mathrm{T}i(+1)}\rangle \approx |\phi^{\mathrm{T}i}_{o\beta\rightarrow v\alpha}\rangle = \frac{1}{\sqrt{N_e!}} \det\Big(\varphi^{\mathrm{T}i}_1\boldsymbol{\alpha}, \varphi^{\mathrm{T}i}_1\boldsymbol{\beta}, \ldots, \varphi^{\mathrm{T}i}_o\boldsymbol{\alpha}, \underline{\varphi^{\mathrm{T}i}_v\boldsymbol{\alpha}}, \ldots, \varphi^{\mathrm{T}i}_{\frac{N_e}{2}}\boldsymbol{\alpha}, \varphi^{\mathrm{T}i}_{\frac{N_e}{2}}\boldsymbol{\beta}\Big), \tag{9}
$$

$$
\begin{aligned}
|\psi^{\mathrm{T}i(0)}\rangle &\approx \frac{1}{\sqrt{2}}\big(|\phi^{\mathrm{T}i}_{o\alpha\rightarrow v\alpha}\rangle - |\phi^{\mathrm{T}i}_{o\beta\rightarrow v\beta}\rangle \big) \\
&= \frac{1}{\sqrt{2N_e!}}\Big\{ \det\Big(\varphi^{\mathrm{T}i}_1\boldsymbol{\alpha}, \varphi^{\mathrm{T}i}_1\boldsymbol{\beta}, \ldots, \underline{\varphi^{\mathrm{T}i}_v\boldsymbol{\alpha}}, \varphi^{\mathrm{T}i}_o\boldsymbol{\beta}, \ldots, \varphi^{\mathrm{T}i}_{\frac{N_e}{2}}\boldsymbol{\alpha}, \varphi^{\mathrm{T}i}_{\frac{N_e}{2}}\boldsymbol{\beta}\Big) - \\
&\qquad \det\Big(\varphi^{\mathrm{T}i}_1\boldsymbol{\alpha}, \varphi^{\mathrm{T}i}_1\boldsymbol{\beta}, \ldots, \varphi^{\mathrm{T}i}_o\boldsymbol{\alpha}, \underline{\varphi^{\mathrm{T}i}_v\boldsymbol{\beta}}, \ldots, \varphi^{\mathrm{T}i}_{\frac{N_e}{2}}\boldsymbol{\alpha}, \varphi^{\mathrm{T}i}_{\frac{N_e}{2}}\boldsymbol{\beta}\Big) \Big\},
\end{aligned} \tag{10}
$$

$$|\psi^{\mathrm{T}i(-1)}\rangle \approx |\phi^{\mathrm{T}i}_{o\alpha\to v\beta}\rangle = \frac{1}{\sqrt{N_e!}} \det\left(\varphi_1^{\mathrm{T}i}\boldsymbol{\alpha}, \varphi_1^{\mathrm{T}i}\boldsymbol{\beta}, \ldots, \underline{\varphi_v^{\mathrm{T}i}\boldsymbol{\beta}}, \varphi_o^{\mathrm{T}i}\boldsymbol{\beta}, \ldots, \varphi_{\frac{N_e}{2}}^{\mathrm{T}i}\boldsymbol{\alpha}, \varphi_{\frac{N_e}{2}}^{\mathrm{T}i}\boldsymbol{\beta}\right), \quad (11)$$

where the spin projection number onto the z axis is indicated within superscript parentheses. Only the states T(+1) or T(−1) are directly obtained from the SCF optimization and their KS orbitals are used to construct the T(0) state. ΔSCF procedures employing the spin purification within RO-KS formulation where the triplet and mixed states with rounded occupations are optimized simultaneously can be also used to construct the aforementioned states (8)–(11).[41,42]

Since all electronic states are obtained independently via ΔSCF, the corresponding KS orbitals are not mutually orthogonal between different electronic states, $\langle\varphi_j^i|\varphi_{j'}^{i'}\rangle \neq \delta_{jj'}$ (where δ is the Kronecker delta). This makes the direct use of approximate wave functions (8)–(11) impractical for the calculation of SOC terms, as the nonorthogonal KS orbitals dismiss the antisymmetric property of the orbital angular momentum terms in equation (3) ($\langle\varphi_i^X|\,\hat{\xi}_j\,|\varphi_k^Y\rangle \neq -\langle\varphi_k^X|\,\hat{\xi}_j\,|\varphi_i^Y\rangle$). To resolve this, the excited electronic states can be represented as a linear combination of configuration state functions (CSFs)

$$|\psi^i\rangle = \sum_{pw} C^i_{pw}\,|\Phi^{\mathrm{S0}}_{p\to w}\rangle + \sum_{pp'ww'} C^i_{pp'ww'}\,|\Phi^{\mathrm{S0}}_{p\to w,p'\to w'}\rangle + \ldots, \quad (12)$$

where all the $|\Phi^{\mathrm{S0}}\rangle$ CSFs are composed of appropriate Slater determinants which are all made of the ground electronic state KS orbitals. C are projections of the $|\psi^i\rangle$ onto CSFs, $C^i_{pp'\ldots ww'\ldots} = \langle\Phi^{\mathrm{S0}}_{p\to w,p'\to w'\ldots}|\psi^i\rangle$, where the index p (and p') goes over all occupied MOs, while w (w') over all available virtual MOs. CSFs constructed from single orbital transition configurations are analogue to the right-hand side expressions (8)–(11) of corresponding spin state, and are sufficient in the expansion (12) for calculating the SOC terms. As the single excitation CSF of singlet multiplicity is $|\Phi^{\mathrm{S0}}_{p\to w}\rangle = (|\phi^{\mathrm{S0}}_{p\alpha\to w\alpha}\rangle + |\phi^{\mathrm{S0}}_{p\beta\to w\beta}\rangle)/\sqrt{2}$, the

approximate singlet wave function (8) takes the form (further designated with the $|\tilde{\psi}\rangle$)

$$|\psi^{\mathrm{S}i}\rangle \approx |\tilde{\psi}^{\mathrm{S}i}\rangle = \frac{1}{\sqrt{2}} \sum_{pw} C_{pw}^{\mathrm{S}i} \big(|\phi^{\mathrm{S0}}_{p\alpha\to w\alpha}\rangle + |\phi^{\mathrm{S0}}_{p\beta\to w\beta}\rangle \big), \tag{13}$$

where the corresponding coefficients are

$$\begin{aligned} C_{pw}^{\mathrm{S}i} =& \frac{1}{2}\Big(\langle\phi^{\mathrm{S0}}_{p\alpha\to w\alpha}|\phi^{\mathrm{S}i}_{o\alpha\to v\alpha}\rangle + \langle\phi^{\mathrm{S0}}_{p\alpha\to w\alpha}|\phi^{\mathrm{S}i}_{o\beta\to v\beta}\rangle + \langle\phi^{\mathrm{S0}}_{p\beta\to w\beta}|\phi^{\mathrm{S}i}_{o\alpha\to v\alpha}\rangle + \langle\phi^{\mathrm{S0}}_{p\beta\to w\beta}|\phi^{\mathrm{S}i}_{o\beta\to v\beta}\rangle \Big) \\ =& \langle\phi^{\mathrm{S0}}_{p\alpha\to w\alpha}|\phi^{\mathrm{S}i}_{o\alpha\to v\alpha}\rangle + \langle\phi^{\mathrm{S0}}_{p\beta\to w\beta}|\phi^{\mathrm{S}i}_{o\alpha\to v\alpha}\rangle\,, \end{aligned} \tag{14}$$

obtained by expanding $\langle\Phi^{\mathrm{S0}}_{p\to w}|\psi^{\mathrm{S}i}\rangle$. Analogously the approximate triplet wave functions (9)–(11) become

$$|\psi^{\mathrm{T}i(+1)}\rangle \approx |\tilde{\psi}^{\mathrm{T}i(+1)}\rangle = \sum_{pw} C_{pw}^{\mathrm{T}i}\, |\phi^{\mathrm{S0}}_{p\beta\to w\alpha}\rangle\,, \tag{15}$$

$$|\psi^{\mathrm{T}i(0)}\rangle \approx |\tilde{\psi}^{\mathrm{T}i(0)}\rangle = \frac{1}{\sqrt{2}} \sum_{pw} C_{pw}^{\mathrm{T}i} \big(|\phi^{\mathrm{S0}}_{p\alpha\to w\alpha}\rangle - |\phi^{\mathrm{S0}}_{p\beta\to w\beta}\rangle \big), \tag{16}$$

$$|\psi^{\mathrm{T}i(-1)}\rangle \approx |\tilde{\psi}^{\mathrm{T}i(-1)}\rangle = \sum_{pw} C_{pw}^{\mathrm{T}i}\, |\phi^{\mathrm{S0}}_{p\alpha\to w\beta}\rangle\,, \tag{17}$$

with corresponding coefficients

$$\begin{aligned} C_{pw}^{\mathrm{T}i} &= \langle\phi^{\mathrm{S0}}_{p\alpha\to w\alpha}|\phi^{\mathrm{T}i}_{o\alpha\to v\alpha}\rangle - \langle\phi^{\mathrm{S0}}_{p\beta\to w\beta}|\phi^{\mathrm{T}i}_{o\alpha\to v\alpha}\rangle \\ &= \langle\phi^{\mathrm{S0}}_{p\beta\to w\alpha}|\phi^{\mathrm{T}i}_{o\beta\to v\alpha}\rangle = \langle\phi^{\mathrm{S0}}_{p\alpha\to w\beta}|\phi^{\mathrm{T}i}_{o\alpha\to v\beta}\rangle\,. \end{aligned} \tag{18}$$

These approximate wave functions (13), (15)–(17) are analogue to TD-DFT auxiliary wave functions[49,61,62,64] or the configuration interaction singles (CIS)[48] and can be used to obtain other observables. For example, the transition dipole moment (TDM) between the ground

and excited singlet electronic states is

$$\begin{aligned}\langle\psi^{\mathrm{S}0}|\,\hat{\boldsymbol{\mu}}\,|\psi^{\mathrm{S}i}\rangle &\approx \langle\phi^{\mathrm{S}0}|\,\hat{\boldsymbol{\mu}}\,|\tilde{\psi}^{\mathrm{S}i}\rangle \\ &= \frac{1}{\sqrt{2}}\sum_{pw} C_{pw}^{\mathrm{S}i}\big(\,\langle\phi^{\mathrm{S}0}|\,\hat{\boldsymbol{\mu}}\,|\phi^{\mathrm{S}0}_{p\alpha\to w\alpha}\rangle + \langle\phi^{\mathrm{S}0}|\,\hat{\boldsymbol{\mu}}\,|\phi^{\mathrm{S}0}_{p\beta\to w\beta}\rangle\,\big) \\ &= \sqrt{2}\sum_{pw} C_{pw}^{\mathrm{S}i}\,\langle\varphi_p^{\mathrm{S}0}|\,\hat{\boldsymbol{\mu}}\,|\varphi_w^{\mathrm{S}0}\rangle\,,\end{aligned} \tag{19}$$

where $\hat{\boldsymbol{\mu}}$ is the TDM vector operator, either in position or velocity representation, which in the first two lines of above expression (19) is an N_e-electron operator, and just a single electron operator in the last line of (19). The last line is obtained by inserting the corresponding Slater determinants into the previous line and integrating over all electrons. Combining the approximate wave functions (13)–(17) with the one-electron SOC operator (2), the one-electron SOC terms between the ground electronic (7) and excited triplet electronic (9)–(11) states are (in atomic units)

$$\langle\psi^{\mathrm{S}0}|\,\hat{H}_{\mathrm{SOC}}\,|\psi^{\mathrm{T}i(0)}\rangle \approx \imath\frac{\alpha^2}{2}\sqrt{2}\sum_{pw} C_{pw}^{\mathrm{T}i}\,\langle\varphi_p^{\mathrm{S}0}|\,\hat{\xi}_z\,|\varphi_w^{\mathrm{S}0}\rangle\,, \tag{20}$$

and

$$\langle\psi^{\mathrm{S}0}|\,\hat{H}_{\mathrm{SOC}}\,|\psi^{\mathrm{T}i(\pm1)}\rangle \approx \imath\frac{\alpha^2}{2}\sum_{pw} C_{pw}^{\mathrm{T}i}\,\langle\varphi_p^{\mathrm{S}0}|\,\hat{\xi}_x \pm \imath\hat{\xi}_y\,|\varphi_w^{\mathrm{S}0}\rangle\,, \tag{21}$$

while between the excited singlet (8) and triplet states they are

$$\begin{aligned}\langle\psi^{\mathrm{S}i}|\,\hat{H}_{\mathrm{SOC}}\,|\psi^{\mathrm{T}j(0)}\rangle \approx \imath\frac{\alpha^2}{2}\Bigg(&\sum_{pww'} C_{pw}^{\mathrm{S}i}C_{pw'}^{\mathrm{T}j}\,\langle\varphi_w^{\mathrm{S}0}|\,\hat{\xi}_z\,|\varphi_{w'}^{\mathrm{S}0}\rangle - \\ &\sum_{pp'w} C_{pw}^{\mathrm{S}i}C_{p'w}^{\mathrm{T}j}\,\langle\varphi_{p'}^{\mathrm{S}0}|\,\hat{\xi}_z\,|\varphi_p^{\mathrm{S}0}\rangle\Bigg),\end{aligned} \tag{22}$$

and

$$\langle\psi^{\mathrm{S}i}|\,\hat{H}_{\mathrm{SOC}}\,|\psi^{\mathrm{T}j(\pm1)}\rangle \approx \imath\frac{\alpha^2}{2^{3/2}}\Bigg(\sum_{pww'} C^{\mathrm{S}i}_{pw}C^{\mathrm{T}j}_{pw'}\,\langle\varphi^{\mathrm{S0}}_{w}|\,\hat{\xi}_x \pm \imath\hat{\xi}_y\,|\varphi^{\mathrm{S0}}_{w'}\rangle - \sum_{pp'w} C^{\mathrm{S}i}_{pw}C^{\mathrm{T}j}_{p'w}\,\langle\varphi^{\mathrm{S0}}_{p'}|\,\hat{\xi}_x \pm \imath\hat{\xi}_y\,|\varphi^{\mathrm{S0}}_{p}\rangle\Bigg). \tag{23}$$

The one-electron SOC terms between different triplet excited states (9)–(11) are

$$\langle\psi^{\mathrm{T}i(0)}|\,\hat{H}_{\mathrm{SOC}}\,|\psi^{\mathrm{T}j(\pm1)}\rangle \approx \mp\imath\frac{\alpha^2}{2^{3/2}}\Bigg(\sum_{pww'} C^{\mathrm{T}i}_{pw}C^{\mathrm{T}j}_{pw'}\,\langle\varphi^{\mathrm{S0}}_{w}|\,\hat{\xi}_x \pm \imath\hat{\xi}_y\,|\varphi^{\mathrm{S0}}_{w'}\rangle - \sum_{pp'w} C^{\mathrm{T}i}_{pw}C^{\mathrm{T}j}_{p'w}\,\langle\varphi^{\mathrm{S0}}_{p'}|\,\hat{\xi}_x \pm \imath\hat{\xi}_y\,|\varphi^{\mathrm{S0}}_{p}\rangle\Bigg). \tag{24}$$

and

$$\langle\psi^{\mathrm{T}i(\pm1)}|\,\hat{H}_{\mathrm{SOC}}\,|\psi^{\mathrm{T}j(\pm1)}\rangle \approx \pm\imath\frac{\alpha^2}{2}\Bigg(\sum_{pww'} C^{\mathrm{T}i}_{pw}C^{\mathrm{T}j}_{pw'}\,\langle\varphi^{\mathrm{S0}}_{w}|\,\hat{\xi}_z\,|\varphi^{\mathrm{S0}}_{w'}\rangle - \sum_{pp'w} C^{\mathrm{T}i}_{pw}C^{\mathrm{T}j}_{p'w}\,\langle\varphi^{\mathrm{S0}}_{p'}|\,\hat{\xi}_z\,|\varphi^{\mathrm{S0}}_{p}\rangle\Bigg). \tag{25}$$

On the other hand, the one-electron SOC terms $\langle\psi^{\mathrm{T}i(0)}|\,\hat{H}_{\mathrm{SOC}}\,|\psi^{\mathrm{T}j(0)}\rangle$ and $\langle\psi^{\mathrm{T}i(\pm1)}|\,\hat{H}_{\mathrm{SOC}}\,|\psi^{\mathrm{T}j(\mp1)}\rangle$ vanish (see Supporting Information for derivation of aforementioned expressions). It should be pointed out that the expansions (13) and (15)–(17) do not alleviate the nonorthogonality between excited electronic states of the same multiplicity, as they are all obtained independently. However, as all states are now constructed from the same set of KS-MOs, the antisymmetric property of all final SOC terms (20)–(25) is restored ($\langle\varphi^{\mathrm{S0}}_{i}|\,\hat{\xi}_j\,|\varphi^{\mathrm{S0}}_{k}\rangle = -\,\langle\varphi^{\mathrm{S0}}_{k}|\,\hat{\xi}_j\,|\varphi^{\mathrm{S0}}_{i}\rangle$), giving expressions that are analogue to reported TD-DFT relations.[51,65] All SOC terms are hermitian, and terms coupling singlet electronic state with the ±1 projections of triplet electronic states (21),(23), T(0) with T(±1) (24), and same ±1 projection pairs of two different triplet electronic states (25) are mutually complex conjugated pairs.

2.2 Incorporation of ΔSCF SOC into trajectory surface hopping

As $\hat{\xi}_x$, $\hat{\xi}_y$, and $\hat{\xi}_z$ are components of the vector $\hat{\boldsymbol{\xi}}$, all aforementioned one-electron SOC terms depend on the orientation of the coordinate system. While a coordinate system can be associated with a molecular frame and held fix,[71] this is not always practical, particularly for large (periodic) systems. Instead, as the norm of vector $\hat{\boldsymbol{\xi}}$ is invariant to rotation, one-electron SOC terms over all degenerate triplet states can be combined into a single one-electron SOC term as[51,72]

$$\langle \psi^{\mathrm{S}i} | \, \hat{H}_{\mathrm{SOC}} \, | \psi^{\mathrm{T}j} \rangle = \left(\sum_{k=+1,0,-1} \left| \langle \psi^{\mathrm{S}i} | \, \hat{H}_{\mathrm{SOC}} \, | \psi^{\mathrm{T}j(k)} \rangle \right|^2 \right)^{1/2} . \tag{26}$$

For one-electron SOC between two triplet states, (24) and (25) are all combined together as above. While this removes the coordinate orientation dependence from the SOC terms, it diminishes the details of population balance between different total spin projections of the degenerate triplet electronic states, which, depending on the choice of SH algorithm, can significantly affect the NA hopping probabilities.[73] Since the NA-MD in a spin-adiabatic states framework as suggested by Granucci *et al.*[73] is not a practical solution due to the lack of electronic gradients of the full electronic SOC Hamiltonian at the ΔSCF level, for the demonstration purposes of SOC terms in NA-MD at the ΔSCF level of theory we remain in the spin-diabatic framework, meaning that electronic states of equal multiplicities are considered adiabatic while pairs of states of different multiplicities are treated as strictly diabatic. With the association of individual SOC terms into one element (26) so are all three triplet degenerate states combined into one electronic state. Due to the lack of phase continuity of such a combined SOC term (26) certain SH schemes, in particular the Tully's fewest-switching surface hopping algorithm[74], are severely affected at strong SOC regions as demonstrated by Granucci and co-authors.[73] On the other hand, the SH probabilities obtained by a standard Landau–Zener (LZ) algorithm are less affected compared to exact quantum solutions even in regions of configuration space with large SOC terms.[73] Hence, an

LZ-SH algorithm in an NA formulation by Belyaev and Lebedev[75] was used to determine the hopping probability $\mathcal{P}$ between states of equal multiplicities

$$\mathcal{P}^{\mathrm{X}i\rightarrow\mathrm{X}j} = \exp\left[-\frac{\pi}{2}\left(\frac{|E^{\mathrm{X}i} - E^{\mathrm{X}j}|^3}{\frac{d^2}{dt^2}|E^{\mathrm{X}i} - E^{\mathrm{X}j}|}\right)^{1/2}\right], \tag{27}$$

while for NA hops between electronic states of different multiplicities the diabatic LZ-SH probability formula is used[76,77]

$$\mathcal{P}^{\mathrm{X}i\rightarrow\mathrm{Y}j} = 1 - \exp\left[-2\pi\frac{|\left\langle\psi^{\mathrm{X}i}\right|\hat{H}_{\mathrm{SOC}}\left|\psi^{\mathrm{Y}j}\right\rangle|^2}{\frac{d}{dt}|E^{\mathrm{X}i} - E^{\mathrm{Y}j}|}\right]. \tag{28}$$

Expression (28) is used only at intersection points between electronic states of different multiplicity. It should be noted that this approximation ignores degeneracy effects and Berry force contribution to the NA-MD which influences the detailed balance and consequentially the branching accuracy and photochemical quantum yields,[78,79] but is sufficient for observing new deactivation mechanisms via intersystem crossings.

Our SH-NA-MD implementation is also equipped with Tully's fewest-switching SH algorithm incorporating SOC terms in an analogue way as Franco de Carvalho and Tavernelli showed for TD-DFT.[76] This is sufficient for elucidating nonradiative deactivation mechanisms undergoing intersystem crossings but due to aforementioned disadvantages of the Tully's SH procedure with SOC inadequate for simulating accurate details of such NA processes. The approximated wave functions (7)–(11) associated with corresponding electronic states are used to calculate the NA coupling terms via the Tully–Hammes-Schiffer formula.[31,80] Their expansions into linear combination of singly-excited CSFs composed of ground electronic state KS-MOs (13) and (15)–(17) can be equally used for determination of NA couplings, eliminating the contribution from the ground electronic states, although the hermitian contribution[31] to the couplings between excited electronic states of same multiplicities remains as the expansion (12) does not mutually orthogonalize excited electronic

states. Generally, as ΔSCF excited electronic states are obtained independently, they are of continuous electronic character and thus behave as diabatic states in this respect, but at the same time they possess NA coupling elements with other electronic states. None of the approximated ΔSCF wave functions (7)–(11) are eigenfunctions of the the total electronic Hamiltonian $\hat{H}_e$, and they do not satisfy the Brillouin's theorem[81,82], because due to their mutual nonorthogonality the off-diagonal Hamiltonian terms $\langle\psi^{\mathrm{S}0}|\,\hat{H}_e\,|\psi^{\mathrm{S}i}\rangle$ between ground and excited electronic states do not vanish. Only by applying the expanded approximated wave functions (13) the off-diagonal terms with the ground electronic state would vanish. Further details on incorporating off-diagonal Hamiltonian and hermitian NA coupling terms into Tully's SH-NA-MD can be found in the papers by Akimov and collaborators,[25,83] which, for the systems studied up to now, can all be safely ignored for the purpose of Tully's SH-NA-MD as demonstrated in our previous work.[31]

Another important detail to account for is the application of hybrid functionals with the singlet excited electronic states constructed with half-occupied occupied (o) and virtual (v) KS-MOs. A corresponding singlet excited electronic state density matrix introduces a $\{(oo|oo)+(vv|vv)\}/2$ term, where generally $(jk|lm) = \int \varphi_j^*(\boldsymbol{r})\varphi_k(\boldsymbol{r})(\boldsymbol{r}-\boldsymbol{r}')^{-1}\varphi_l^*(\boldsymbol{r}')\varphi_m(\boldsymbol{r}')d\boldsymbol{r}d\boldsymbol{r}'$, into the Coulomb energy but only half of this value into the exact exchange part of the energy. This is derived from the density matrix expressions for the Coulomb and exact Hartree–Fock exchange energy terms.[84] The former energy term contributes to the self-interaction error[85,86] that cannot be fully annihilated by the latter exact Hartree–Fock exchange (since it is only half of the former value when 100% of exact Hartree–Fock exchange is included), therefore by including a contribution of the exact Hartree–Fock exchange to the xc functional, a shift of the singlet excited electronic state energy is caused due to the inadequately accounted self-interaction error. Since the exchange functional part is reduced by the fraction of the exact Hartree–Fock exchange, the shift increases almost linearly with the fraction of the exact Hartree–Fock exchange in the hybrid functional. This behaviour is similar to the reported case of the ground electronic state energies with increasing contributions of the exact

Hartree–Fock exchange in the H_2^+ system.[87] Although an artifact, KS half-occupied o and v MOs do not change significantly over a wide range of configuration space due to which the shift is almost constant (as shown later), and as their change is very slow the shift does not significantly influence the nuclear gradients of the singlet excited electronic potential energy surface. To reduce its effect on NA-MD, it is possible to shift the singlet excited state energies by a constant value, predetermined from preliminary excited state analysis or preliminary trajectories, or reduce the contribution of the exact Hartree–Fock exchange in hybrid functionals. We have previously demonstrated the capabilities of NA-MD with the blueshifted S1 electronic state.[31] The triplet excited electronic states T($\pm$1) possess corresponding density matrices only with integer occupations which adequately alleviate this additional contribution to the self-interaction error.

3 Computational Details

A modified version of the CP2K code[88] in which the occupations of each spin set of KS-MOs can be manipulated was used for all ΔSCF calculations. The RO-KS formulation was employed for the computation of all singlet and triplet excited electronic states. The PBE0[89] functional with the auxiliary density matrix method (ADMM) and the cFIT3 auxiliary basis set[90] was combined with the all-electron def2-TZVP[91], or the TZVP-GTH basis set[92] for which the Goedecker–Teter–Hutter (GTH) pseudopotentials[93] were applied. For calculations with the PBE functional[94,95] the all-electron Pople-style 6-31G(d) basis set[96–98] was used. In both types of calculations, the plane wave cutoff was set to 500 Ry.

The angular momentum operator terms (3) for each atom were also computed with the CP2K code and, together with the KS-MOs used to calculate the one-electron SOC terms according to the aforementioned theory. Even though when applying pseudopotentials with CP2K the nuclear charges are reduced by the the number of electrons each corresponding pseudopotential substitutes, for the calculations of SOC terms full nuclear charge of corre-

sponding atoms were used. The procedure was implemented into an in-house Python script that is an interface between CP2K and a modified version of the Zagreb Surface Hopping code[99–101] which was extended to include the NA-MD of triplet excited electronic states.

The same in-house Python script was used for the calculation of electronic TDMs, both in length and velocity representations. For all examined ΔSCF excited electronic states, the occupied-unoccupied KS-MO pair for the construction of the single reference determinants was directly determined from the TD-DFT largest transition amplitude for each excited state.

The nuclear trajectory for NA-MD was propagated with the velocity Verlet's algorithm in time steps of 0.5 fs. NA hops between the electronic states were conducted with the LZ-SH algorithm. Velocities were rescaled uniformly after the NA hop to preserve the total energy. The system's initial conditions were sampled from a thermalized Wigner distribution function, for which the corresponding normal modes were extracted from CP2K computed Hessian.[31]

For comparison, the one-electron SOC and TDM terms were recomputed at the Tamm–Dancoff LR-TD-DFT level[65] as implemented in the Orca program package.[102,103] Again, the PBE exchange–correlation functional was paired with the 6-31G(d) basis set and PBE0 with the def2-TZVP[91] basis set. The same nuclear charges were used as for CP2K calculations.

Molecules thioformaldehyde, cyclopropanone, uracil, *p*-nitrophenol, and TATA+ were optimized in the ground electronic state at the PBE/6-31G(d) level of theory using the CP2K program package without any symmetry constrains.

4 Results

4.1 Spin-orbit couplings

In the Franck–Condon region, formaldehyde's first singlet electronic excited state, further designated as S1, is of $n \rightarrow \pi^*$ character and is encased from below by the first triplet

state (T1) of the same character, while on top by the second triplet excited state (T2) of $\pi \rightarrow \pi^*$ character. Due to the antibonding character of the S1 excited state, its corresponding potential energy surface has a local minimum structure with an elongated C=O bond and a pyramidalized C atom. A similar minimum exists on the T1 potential energy surface. To benchmark the one-electron SOC terms at the ΔSCF level, several structures were computed with a contracted/extended C=O bond from the ground electronic state minimum structure and compared to the TD-DFT reference results. Fig. 1a displays the energy profiles of the aforementioned states computed at the PBE/6-31G(d) level of theory, while Fig. 1c shows the values computed at the PBE0/def2-TZVP level.

Around the minimum geometry the ΔSCF excited electronic states are all blueshifted compared to the TD-DFT curves but follow the same trend as the ones from TD-DFT (Fig. 1a and c). While the triplet states are shifted less, the singlet states display more offset, particularly the S1 ΔSCF PBE0/def2-TZVP state due to the contribution form the exact Hartree–Fock exchange. From about -0.2 a_0 contracted to the maximum displayed extension of 1.35 a_0, for the relative change of C=O bond length, the ΔSCF PBE0/def2-TZVP S1 electronic state is shifted almost constantly by ∼1.7 eV from the corresponding TD-DFT S1 curve. In the region of extreme C=O bond contraction the ΔSCF values are significantly redshifted (not shown). The slight asymmetry of all the states computed at the PBE0/def2-TZVP level with CP2K DFT and ΔSCF methods, compared to the TD-DFT curves, is due to the ADMM used with CP2K,[90] as the calculations without ADMM do not show this asymmetry. The ΔSCF one-electron SOC between the S0 and T1 states accurately matches the corresponding TD-DFT term (Fig. 1b and d), while the S1–T2 SOC term is slightly undervalued at the ΔSCF level. The latter is due to the difference in the coefficients of the single-excitation determinants (14) and (18) when compared to the corresponding counterpart transition amplitudes of TD-DFT, while the orbital angular momentum terms are identical between the two codes. Other one-electron SOC coupling terms for the listed states are insignificant (with values $< 10^{-4}$ cm^{-1}) and contaminated with noise for both

methods, they are therefore omitted.

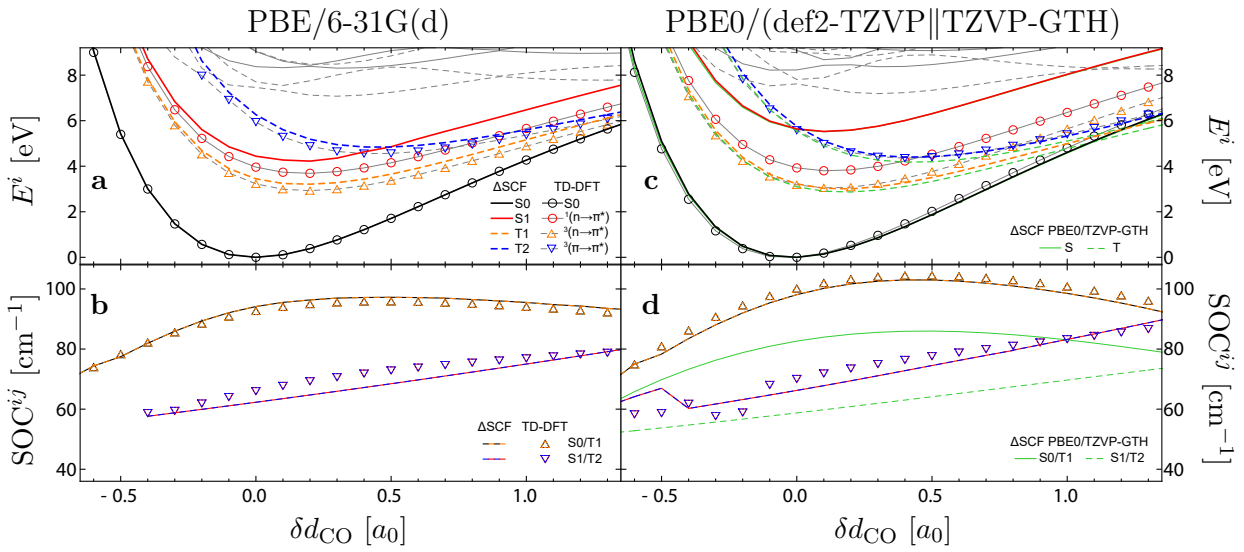

Figure 1: Energy profile of several singlet (full lines) and triplet (dashed lines) electronic states along the relative change of the C=O bond length (δd_{CO}, in Bohr units) in formaldehyde. 0.0 corresponds to the ground state equilibrium bond length. In plots **a** and **c** black, red, orange, and blue color lines indicate S0, S1, T1, and T2 ΔSCF electronic states, respectively. Gray lines indicate adiabatic TD-DFT electronic states, where the black and red circles trace the singlet ground and $^1(n \rightarrow \pi^*)$ characters, respectively, while orange and blue triangles the triplet $^3(n \rightarrow \pi^*)$ and $^3(\pi \rightarrow \pi^*)$ characters, respectively. Plots **b** and **d** show the one-electron SOC terms between S0 and T1 electronic states (in black-orange colors), and between S1 and T2 (in red-blue colors). Full lines indicate ΔSCF, while triangles trace out the TD-DFT values. All values in plots a and b were obtained using the PBE exchange–correlation functional with the 6-31G(d) basis set. In figures **c** and **d** the PBE0 functional was combined with the all-electron def2-TZVP basis set, or with the TZVP-GTH basis set used exclusively with the ΔSCF method. Corresponding values computed with the TZVP-GTH basis set are indicated by green lines in figures **c** and **d** and are paired with the corresponding all-electron counter curves.

The green curves in Fig. 1c represent the same energy profile but computed with the PBE0 functional and a TZVP-GTH[92] basis set for CP2K ΔSCF, which employs the GTH pseudopotentials[93], commonly used for Gaussian and plane wave (GPW) calculations in CP2K. T1 and T2 ΔSCF energies obtained using the GTH pseudopotentials are slightly red shifted compared to the all-electron ΔSCF counter values. The one-electron SOC terms determined at the ΔSCF PBE0/TZVP-GTH level are smaller by a factor of 1.22 ± 0.06 compared to the all-electron ΔSCF or TD-DFT counter values obtained with the same

functional. Trends are, however, the same. The main reason for this discrepancy lays in the difference of the angular momentum terms (3) between the two basis sets, as the main contributing terms to the SOCs are all smaller for the TZVP-GTH basis set. Fig. 1c also demonstrates the diabatic nature of the ΔSCF states, since it was only required to converge the same corresponding excited state electron density for each electronic state. To obtain smooth TD-DFT one-electron SOC curves, it was necessary to patch different adiabatic TD-DFT states of the same character by properly connecting the states along the entire energy profile.

The observed trends are also preserved along an NA-MD propagated trajectory. In Fig. 2 electronic state energies and one-electron SOC terms are compared between the original DFT/ΔSCF values used to propagate the trajectory, and recalculated DFT/TD-DFT values on the same geometries, where the all-electron def2-TZVP basis set with the PBE0 functional was used.

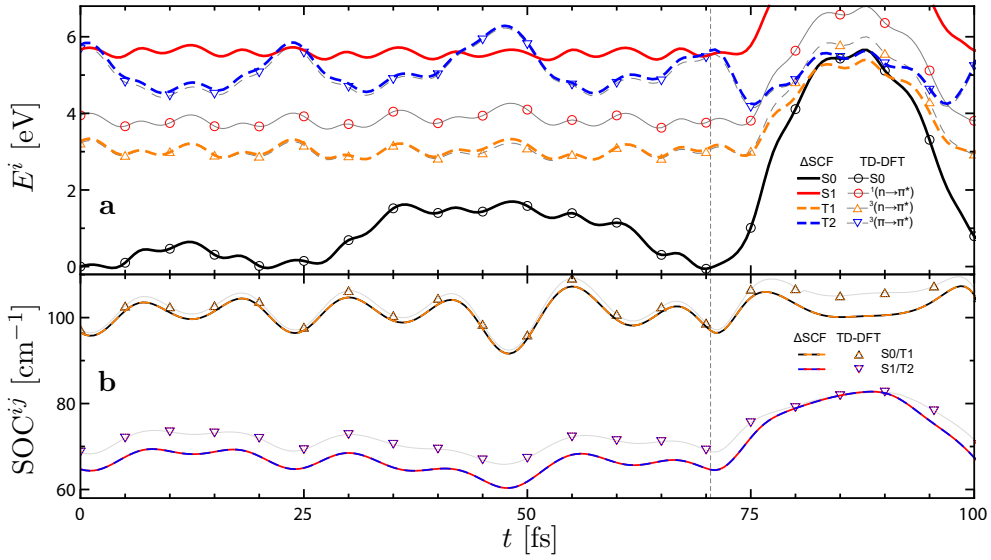

Figure 2: NA-MD trajectory obtained with the DFT/ΔSCF method at the PBE0/def2-TZVP level for formaldehyde initiated in the S1 electronic state. The vertical dashed line indicates the point of intersystem crossing. Figure **a** shows all considered electronic states and figure **b** the corresponding SOC terms. All designations are explained in the caption of Fig. 1.

The NA-MD trajectory is evolved in the initial S1 electronic state until 70.5 fs time mark where the system exhibited intersystem crossing to the T2 electronic state and continues to evolve along it. As the trajectory just further continues to propagate along the T2 electronic state, only the first 100 fs of dynamics are shown. Since the initial part is evolved in the ΔSCF S1 electronic state, trends observed on Fig. 1c are reproduced. Notably, the S1 ΔSCF state exhibits a constant 1.7 eV blueshift relative to the TD-DFT S1 state, but otherwise their topologies are equal. The shapes of the ΔSCF T1 and T2 electronic states potential energy curves deviate more from the TD-DFT values when the C=O bond is extended, as observed in Fig. 1c. This is particularly exhibited between 80 and 93 fs time marks as the TD-DFT triplet electronic states change ordering, i.e., triplet $\pi \rightarrow \pi^*$ character drops in energy under the triplet $n \rightarrow \pi^*$ electronic state. However, the ΔSCF triplet electronic states preserve their original ordering, as they still do not display mutual crossing at these C=O bond extensions. The S1 electronic state blueshift is the reason for the intersystem crossing, as it moves the intersection between S1 and T2 electronic states from 0.45 a_0 (relative C=O bond change) to ∼0 a_0 (as shown in Fig. 1). As, due to the blueshift, the trajectory is transferred onto the steep part of the T2 electronic state (instead of the shallow part where crossing occurs at TD-DFT level), the C=O bond is immediately extended, consequentially increasing all energy values. The ΔSCF SOC terms display the same behavior, that is, matching S1/T2 reference values more closer and S0/T1 less for larger C=O bond extensions, as already displayed in Fig. 1. Trajectory in Fig. 2 should be therefore considered just for demonstrating purposes of intersystem crossing at the ΔSCF level, as the S1 electronic state significantly deviates from reference value, inhibiting its use for NA-MD without a priori S1 electronic state shift correction. Regarding computational demands, each SCF cycle takes equal amount of time for the excited electronic state as for the ground electronic state. While the current ΔSCF implementation conducts each excited electronic state calculation separately, TD-DFT calculations of a smaller number of excited electronic states, particularly for such a small system, are faster. In condensed phase systems, however, TD-DFT might require to

calculate a significantly larger number of excited electronic states in dense manifolds just to obtain the properties of the excited electronic state of interest (because it might be positioned higher in energy than other excitations irrelevant to NA-MD), while the ΔSCF selectively calculates the excited electronic state of interest and avoids determining other less important electronic excitations.

Table 1 lists combined one-electron SOC terms (26) between S0, S1, S2 singlet, and T1 and T2 triplet electronic states for a selection of larger molecules. All values are determined at the DFT/ΔSCF PBE/6-31G(d) level of theory and compared to TD-DFT reference values computed with the same functional and basis set. These molecules and states were chosen as they are all of single reference characters at the TD-DFT level of theory. In fact, all the TD-DFT transition amplitudes (more precisely their squares X_{ov}^2) for each of their single dominating $o \rightarrow v$ transition in all listed electronic states are 0.9 or larger. Since all orbital angular moment terms (3) are equal between the two methods, differences arise from the contributions of the singly-excited Slater determinants for each excited electronic state, (14) and (18). Although not perfect, ΔSCF SOCs between ground and excited triplet electronic states match well the reference values. Slightly larger discrepancies are observed for some ΔSCF SOCs between excited singlet and triplet electronic states compared to reference, as the differences in approximate wave function expansion coefficients $C_{ov}^{\mathrm{S}i}$ and $C_{ov}^{\mathrm{T}i}$ accumulate more in these terms, (22)–(23). This is especially noticeable for S2/Ti SOCs in uracil and *p*-nitrophenol, where in both cases their S2 electronic states when expanded into linear combination of singly-excited Slater determinants (13) possess the square of the dominating coefficient C_{max}^{S2} of the order of 0.7, while for all other states and molecules the square of the dominating coefficients are ∼0.9 or larger. It should be noted that in all listed states, the sum of all squares of coefficients associated to each singly-excited Slater determinants are ∼99%, with less then 1 permille remaining for the contribution of multiple-excited Slater determinants.

Table 1: Combined one-electron SOC terms (as defined by equation (26)) for a number of molecules and up to the second singlet and triplet excited electronic state computed at the DFT/ΔSCF PBE/6-31G(d) level of theory. Reference values in parenthesis are determined with the same functional and basis set using the TD-DFT method. All values are in cm^{-1}.

	Thioformaldehyde		Cyclopropanone		Uracil		*p*-Nitrophenol		TATA+	
	T1	T2	T1	T2	T1	T2	T1	T2	T1	T2
S0	221.5	0.0	78.7	47.2	1.8	63.4	0.0	76.2	0.0	0.1
	(220.5)	(0.0)	(79.5)	(36.0)	(1.8)	(56.8)	(0.0)	(71.1)	(0.0)	(0.0)
S1	0.0	159.0	0.0	49.2	28.9	0.5	15.3	0.1	0.2	0.4
	(0.0)	(164.6)	(0.0)	(40.7)	(34.0)	(1.8)	(17.3)	(0.1)	(0.0)	(0.5)
S2	64.6	0.0	50.0	0.0	6.6	26.4	16.7	41.2	0.3	0.0
	(55.4)	(2.0)	(39.0)	(0.0)	(19.3)	(15.2)	(22.5)	(51.3)	(0.5)	(0.0)

4.2 Transition dipole moments

Tables 2, 3, and 4 compare the ΔSCF evaluated TDMs with analogous TD-DFT values, where the first two were determined at the all-electron PBE/6-31G(d) and PBE0/def2-TZVP levels, respectively, while the last at the PBE0 level utilizes the TZVP-GTH basis set with GTH pseudopotentials for the ΔSCF methods. TDMs were computed on an optimized but non-symmetric (C_1) geometry very close to the formaldehyde ground state C_{2v} minimum energy structure so that they do not vanish due to symmetry reasons. Whenever the reference TD-DFT excited state is dominated by a single reference transition, a good match is observed with the ΔSCF value, as expected due to the single reference construction of the latter. In such cases, the vectors are perfectly collinear and their norms are equal in magnitudes.

A significant discrepancy is observed for the S5 state, which at the TD-DFT level is comprised of the Rydberg $n \rightarrow 3p_z$ and valence $\pi \rightarrow \pi^*$ transitions with contributions of 0.518 and 0.440, respectively, as obtained from corresponding TD-DFT transition amplitudes (X_{ov}^2). On the other hand, the RO-KS ΔSCF with rounded occupations only constructs the pure Rydberg transition, as selected based on the largest contribution from the squared TD-DFT amplitudes. Because the TDM vectors of the pure ΔSCF $n \rightarrow 3p_z$ and $\pi \rightarrow \pi^*$ excitations coincide in direction, the ΔSCF TDM appears collinear with the TD-DFT TDM

vector. Discarding the inner shell electrons does not significantly influence the TDM obtained with pseudopotentials as the results in Table 4 demonstrate.

Table 2: Comparison between TD-DFT and ΔSCF computed transition dipole moments (TDMs) at the PBE/6-31G(d) level of theory for the first six singlet formaldehyde excitations. Only the norms of the TDM vectors of length (l.) and velocity (v.) operators are displayed (in atomic units). ΔE indicates the vertical excitation energies for the two methods (in eV). The largest square of the transition amplitudes for each TD-DFT excitation is given in the X^2_{max} column, which also determines the character of the excited state (displayed as the occupied–virtual KS orbital pair in parenthesis in the first column). These orbitals make the dominating single-excitation determinant of the approximated CIS expansion of each ΔSCF excited states, whose largest square of coefficients are given under C^2_{max}. The $\cos\theta$ originates from the dot product between the corresponding normalized ΔSCF TDM vector and the reference TD-DFT TDM vector of the same excitation.

	TD-DFT				ΔSCF					
Si ($\varphi_o \to \varphi_v$)	ΔE	X^2_{max}	TDM l.	TDM v.	ΔE	C^2_{max}	TDM l.	$\cos\theta$	TDM v.	$\cos\theta$
S1 ($n \to \pi^*$)	3.972	0.999	$3.3 \cdot 10^{-4}$	$3.5 \cdot 10^{-4}$	4.423	0.990	$1.7 \cdot 10^{-4}$	1.000	$4.1 \cdot 10^{-6}$	1.000
S2 ($n \to 3s$)	8.377	0.985	$8.7 \cdot 10^{-1}$	$1.6 \cdot 10^{-1}$	9.058	0.951	$1.3 \cdot 10^{0}$	1.000	$4.0 \cdot 10^{-1}$	1.000
S3†($\sigma_{CO} \to \pi^*$)	9.058	0.993	$9.7 \cdot 10^{-2}$	$1.1 \cdot 10^{-3}$	9.321	0.966	$6.7 \cdot 10^{-3}$	1.000	$4.0 \cdot 10^{-3}$	1.000
S4 ($\sigma_{CH} \to \pi^*$)	9.857	0.999	$2.2 \cdot 10^{-4}$	$1.6 \cdot 10^{-4}$	10.290	0.986	$7.0 \cdot 10^{-4}$	1.000	$2.1 \cdot 10^{-4}$	1.000
S5 ($n \to 3p_x$)	9.946	0.518	$1.2 \cdot 10^{-2}$	$1.3 \cdot 10^{-1}$	10.912	0.963	$1.4 \cdot 10^{0}$	0.961	$5.5 \cdot 10^{-1}$	1.000
S6 ($n \to 3p_z$)	11.300	0.996	$1.5 \cdot 10^{-1}$	$1.2 \cdot 10^{-1}$	11.641	0.986	$3.5 \cdot 10^{-2}$	0.999	$4.5 \cdot 10^{-2}$	1.000

† ΔSCF energy converged only up to 10^{-5} instead of 10^{-7} Hartree.

Table 3: Comparison between TD-DFT and ΔSCF computed TDMs at the PBE0/def2-TZVP level of theory for the first three singlet excitations in formaldehyde. Further details are explained in the caption of Table 2.

	TD-DFT				ΔSCF					
Si ($\varphi_o \to \varphi_v$)	ΔE	X^2_{max}	TDM l.	TDM v.	ΔE	C^2_{max}	TDM l.	$\cos\theta$	TDM v.	$\cos\theta$
S1 ($n \to \pi^*$)	4.050	0.995	$3.3 \cdot 10^{-6}$	$3.4 \cdot 10^{-7}$	5.739	0.996	$1.9 \cdot 10^{-6}$	0.281	$2.0 \cdot 10^{-7}$	0.728
S2 ($n \to 3s$)	8.211	0.983	$7.6 \cdot 10^{-1}$	$1.7 \cdot 10^{-1}$	9.758	0.968	$1.0 \cdot 10^{0}$	1.000	$3.1 \cdot 10^{-1}$	1.000
S3 ($\sigma_{CO} \to \pi^*$)	9.335	0.992	$6.8 \cdot 10^{-2}$	$8.3 \cdot 10^{-3}$	10.903	0.976	$4.8 \cdot 10^{-1}$	1.000	$2.5 \cdot 10^{-2}$	1.000

Table 4: Comparison between TD-DFT and ΔSCF computed TDMs at the PBE0 level of theory for the first three singlet excitations in formaldehyde. The TD-DFT method utilizes the all-electron TZVP basis set,[91] while ΔSCF TZVP-GTH with GTH pseudopotentials.[92,93] Further details are explained in the caption of Table 2.

	TD-DFT				ΔSCF					
Si ($\varphi_o \to \varphi_v$)	ΔE	X^2_{max}	TDM l.	TDM v.	ΔE	C^2_{max}	TDM l.	$\cos\theta$	TDM v.	$\cos\theta$
S1 ($n \to \pi^*$)	4.050	0.995	$3.3 \cdot 10^{-6}$	$3.4 \cdot 10^{-7}$	5.714	0.996	$1.9 \cdot 10^{-6}$	0.356	$3.1 \cdot 10^{-7}$	0.731
S2 ($n \to 3s$)	8.211	0.983	$7.6 \cdot 10^{-1}$	$1.7 \cdot 10^{-1}$	10.426	0.588	$5.1 \cdot 10^{-1}$	1.000	$1.6 \cdot 10^{-1}$	1.000
S3 ($\sigma_{CO} \to \pi^*$)	9.335	0.992	$6.8 \cdot 10^{-2}$	$8.3 \cdot 10^{-3}$	10.883	0.975	$5.3 \cdot 10^{-2}$	1.000	$1.7 \cdot 10^{-2}$	1.000

5 Discussion and Conclusions

A procedure for the evaluation of spin-orbit coupling (SOC) between singlet and triplet (excited) electronic states at the ΔSCF level of theory has been introduced. Given that the excited electronic states at the ΔSCF level are independently obtained as optimized excited electronic state densities corresponding to each electronic state, the evaluation of operators coupling two states, equal or different in multiplicities, is not straightforward. Narrowing the procedure to the excited electronic states whose excitation characters are single reference, an approximated mapping from an excited electronic state density onto a singly-excited Slater determinant can be recognized. Viewed in reverse, a singly-excited Slater determinant gives a unique total excited state electron density and establishes a one-to-one relationship between such type of system electronic wave function and its corresponding total electron density. This gives the basis and justification why the ΔSCF method applied here uses exclusively integer and half-integer (1/2) occupation numbers in its final construction of the excited electronic state density for the singlet and triplet states. Such final optimized electron density is not the exact excited electronic state density, but the best approximation which also has a simple corresponding Slater determinant that enables other observables to be computed in addition to the total system's energy, gradient, and few other observables directly available from the corresponding DFT calculations. Furthermore, the construction of states with specific spin multiplicities, here singlet and triplet, requires that the total α and β electron spin densities satisfy certain symmetry relations as well as that these relations are also reflected in their associated Slater determinants. This is because the total spin operator, which is an N_e-electron function operator, has no equal counterpart in DFT as the total density of each spin channel is described by just a single position variable, and cannot uniquely encode as much information as a wave function can. This is clearly observed for the singlet and the triplet states with $S_{tot.,z} = 0$ total spin projection which have the total spin numbers of 0 and 1, respectively, and identical total electron densities for both spin channels. Since the exchange–correlation functional cannot discern between such electronic densities,

their distinction has to be enforced a priori. For this reason, the total electronic density which has a vanishing difference between the two spin densities is strictly associated with a singlet electronic state, while the triplet state with $S_{tot.,z} = 0$ projection has to be constructed from the two triplet states with $S_{tot.,z} \pm 1$ total spin projections as their corresponding electron spin densities are associated with proper triplet states. These spin density symmetry requirements are manifested in the spatial part of the KS orbitals, and to satisfy them the KS spatial orbitals have to be identical between the two spin channels, making the restricted and open-restricted formulations the best choice for their proper construction. The unrestricted KS spin densities can be symmetrical, but there is no strict requirement fur such mutual relation. Whenever this symmetry is compromised, the state is immediately impure with contributions from higher spin multiplicities.

Because of the nonorthogonality of the ΔSCF associated Slater determinants encountered in the construction of observables between different pairs of electronic states, an expansion of the Slater determinant of one state using KS orbitals from the other state removes the nonorthogonal contributions between the two states. To have a consistent basis for such expansion, the ground electronic state KS orbitals were chosen as reference, and the excited state Slater determinants expanded with them. The expansion is complete in the limit of full CI expansion and the complete basis set, but a linear combination of singly-excited Slater determinants constructed from ground state KS orbitals is sufficient to approximate the single reference excited electronic states. It should be noted that this is only an approximation made to obtain observables, not an intended reconstruction of an excited state wave function in form of KS ground electronic state orbitals, and remains mathematically unjustified. However, it bears analogies to the auxiliary wave functions concept encountered in observable computations within LR-TD-DFT. This is further enhanced by the similarity of calculated observables at the ΔSCF level with respect to TD-DFT values.

Under these assumptions, we have implemented the RO-KS single reference excited states into the CP2K program package for the description of excited singlet and triplet electronic

states and used them for the construction of the one-electron SOC terms between these states at the ΔSCF level. They were computed for an isolated formaldehyde molecule and compared to computed TD-DFT values with the Orca software. Almost identical values are obtained if the used basis set between the two codes are equal, while lower CP2K values are obtained as soon as the basis set with pseudopotentials is used instead, but preserving the overall trend of the reference values. This enabled us to run the NA-MD utilizing one-electron SOC terms between singlet and triplet electronic states at the ΔSCF level. In a completely similar manner transition dipole moments were computed between the ground and excited singlet states at the ΔSCF level and, in addition to here, were already applied for the calculation of water solvated cyclopropanone's and its hydrate's absorption spectra.[33] Other observables can be determined in an identical way and might be elucidated in more detail in the future.

Acknowledgement

The work has been supported by the University of Zurich and the Swiss National Science Foundation (grant no. PP00P2 170667). We thank the Swiss National Supercomputing Center for computing resources (project IDs: s875, s1001, and s1036).

Supporting Information Available

Derivation of spin-orbit coupling expressions. This material is available free of charge via the Internet at http://pubs.acs.org.

References

(1) Marian, C.; Schneider, F.; Kleinschmidt, M.; Tatchen, J. Electronic excitation and singlet-triplet coupling in uracil tautomers and uracil-water complexes. *Eur. Phys. J.*

D **2002**, *20*, 357–367.

(2) Perun, S.; Tatchen, J.; Marian, C. M. Singlet and Triplet Excited States and Intersystem Crossing in Free-Base Porphyrin: TDDFT and DFT/MRCI Study. *ChemPhysChem* **2008**, *9*, 282–292.

(3) Effect of H2 binding on the nonadiabatic transition probability between singlet and triplet states of the [NiFe]-Hydrogenase active site. *J. Phys. Chem. A* **2015**, *119*, 1066–1073.

(4) Minaev, B. F.; Ågren, H.; Minaeva, V. A. *Handbook of Computational Chemistry :*; Springer International Publishing, 2017; pp 1557–1587, QC 20181218.

(5) Gozem, S.; Luk, H. L.; Schapiro, I.; Olivucci, M. Theory and Simulation of the Ultrafast Double-Bond Isomerization of Biological Chromophores. *Chem. Rev.* **2017**, *117*, 13502–13565.

(6) Chemi- and Bioluminescence of Cyclic Peroxides. *Chem. Rev.* **2018**, *118*, 6927–6974.

(7) Salazar, S. V.; Mujica, V.; Medina, E. Spin-orbit coupling modulation in DNA by mechanical deformations. *Chimia* **2018**, *72*, 411–417.

(8) Xiao, L.; Chen, Z.; Qu, B.; Luo, J.; Kong, S.; Gong, Q.; Kido, J. Recent progresses on materials for electrophosphorescent organic light-emitting devices. *Adv. Mater.* **2011**, *23*, 926–952.

(9) Minaev, B.; Baryshnikov, G.; Agren, H. Principles of phosphorescent organic light emitting devices. *Phys. Chem. Chem. Phys.* **2014**, *16*.

(10) Mauro, M. Phosphorescent multinuclear complexes for optoelectronics: tuning of the excited-state dynamics. *Chem. Commun.* **2021**, *57*.

(11) Marian, C. M. Understanding and Controlling Intersystem Crossing in Molecules. *Annu. Rev. Phys. Chem.* **2021**, *72*.

(12) Thom, K. A.; Wieser, F.; Diestelhorst, K.; Reiffers, A.; Czekelius, C.; Kleinschmidt, M.; Bracker, M.; Marian, C. M.; Gilch, P. Acridones: Strongly Emissive HIGHrISC Fluorophores. *J. Phys. Chem. Lett.* **2021**, *12*, 5703–5709.

(13) Lee, Y. H.; Shin, Y.-S.; Lee, T.; Jung, J.; Lee, J.-H.; Lee, M. H. Managing local triplet excited states of boron-based TADF emitters for fast spin-flip process: Toward highly efficient TADF-OLEDs with low efficiency roll-off. *Chem. Eng. J.* **2021**, *423*, 130224.

(14) Allison, R. R.; Sibata, C. H. Oncologic photodynamic therapy photosensitizers: A clinical review. *Photodiagnosis Photodyn. Ther.* **2010**, *7*, 61–75.

(15) Kamkaew, A.; Lim, S. H.; Lee, H. B.; Kiew, L. V.; Chung, L. Y.; Burgess, K. BODIPY dyes in photodynamic therapy. *Chem. Soc. Rev.* **2013**, *42*, 77–88.

(16) New avenues in the design and potential application of metal complexes for photodynamic therapy. *RSC Adv.* **2013**, *3*, 25550–25564.

(17) Imberti, C.; Zhang, P.; Huang, H.; Sadler, P. J. New Designs for Phototherapeutic Transition Metal Complexes. *Angew. Chem. Int. Ed.* **2020**, *59*.

(18) Dong, Y.; Kumar, P.; Maity, P.; Kurganskii, I.; Li, S.; Elmali, A.; Zhao, J.; Escudero, D.; Wu, H.; Karatay, A.; Mohammed, O. F.; Fedin, M. Twisted BODIPY derivative: intersystem crossing, electron spin polarization and application as a novel photodynamic therapy reagent. *Phys. Chem. Chem. Phys.* **2021**, *23*, 8641–8652.

(19) Ziegler, T.; Rauk, A.; Baerends, E. J. On the calculation of multiplet energies by the Hartree-Fock-Slater method. *Theor. Chim. Acta* **1977**, *43*, 261–271.

(20) Jones, R. O.; Gunnarsson, O. The density functional formalism, its applications and prospects. *Rev. Mod. Phys.* **1989**, *61*, 689–746.

(21) Hellman, A.; Razaznejad, B.; Lundqvist, B. Potential-energy surfaces for excited states in extended systems. *J. Chem. Phys.* **2004**, *120*, 4593–4602.

(22) Gavnholt, J.; Olsen, T.; Engelund, M.; Schiøtz, J. Δ self-consistent field method to obtain potential energy surfaces of excited molecules on surfaces. *Phys. Rev. B* **2008**, *78*, 075441.

(23) Ziegler, T.; Seth, M.; Krykunov, M.; Autschbach, J.; Wang, F. On the relation between time-dependent and variational density functional theory approaches for the determination of excitation energies and transition moments. *J. Chem. Phys.* **2009**, *130*, 154102.

(24) Maurer, R. J.; Reuter, K. Excited-state potential-energy surfaces of metal-adsorbed organic molecules from linear expansion Δ-self-consistent field density-functional theory (ΔSCF-DFT). *J. Chem. Phys.* **2013**, *139*, 014708.

(25) Pradhan, E.; Sato, K.; Akimov, A. V. Non-adiabatic molecular dynamics with ΔSCF excited states. *J. Condens. Matter Phys.* **2018**, *30*, 484002.

(26) Levi, G.; Ivanov, A. V.; Jónsson, H. Variational Density Functional Calculations of Excited States via Direct Optimization. *J. Chem. Theory Comput.* **2020**, 6968–6982.

(27) Kunze, L.; Hansen, A.; Grimme, S.; Mewes, J.-M. PCM-ROKS for the Description of Charge-Transfer States in Solution: Singlet–Triplet Gaps with Chemical Accuracy from Open-Shell Kohn–Sham Reaction-Field Calculations. *J. Phys. Chem. Lett.* **2021**, *12*, 8470–8480.

(28) Vandaele, E.; Mališ, M.; Luber, S. The ΔSCF method for non-adiabatic dynamics of systems in the liquid phase. *J. Chem. Phys.* **2022**, *156*, 130901.

(29) Lin, M.-F.; Kochat, V.; Krishnamoorthy, A.; Bassman, L.; Weninger, C.; Zheng, Q.; Zhang, X.; Apte, A.; Tiwary, C. S.; Shen, X.; Li, R.; Kalia, R.; Ajayan, P.; Nakano, A.; Vashishta, P.; Shimojo, F.; Wang, X.; Fritz, D. M.; Bergmann, U. Ultrafast non-radiative dynamics of atomically thin MoSe2. *Nat. Commun.* **2017**, *8*, 1745.

(30) Bassman, L.; Krishnamoorthy, A.; Kumazoe, H.; Misawa, M.; Shimojo, F.; Kalia, R. K.; Nakano, A.; Vashishta, P. Electronic Origin of Optically-Induced Sub-Picosecond Lattice Dynamics in $MoSe_2$ Monolayer. *Nano Lett.* **2018**, *18*, 4653–4658.

(31) Mališ, M.; Luber, S. Trajectory Surface Hopping Nonadiabatic Molecular Dynamics with Kohn–Sham ΔSCF for Condensed-Phase Systems. *J. Chem. Theory Comput.* **2020**, *16*, 4071–4086.

(32) Mališ, M.; Luber, S. ΔSCF with Subsystem Density Embedding for Efficient Nonadiabatic Molecular Dynamics in Condensed-Phase Systems. *J. Chem. Theory Comput.* **2021**, *17*, 1653–1661.

(33) Vandaele, E.; Mališ, M.; Luber, S. The photodissociation of solvated cyclopropanone and its hydrate explored via non-adiabatic molecular dynamics using ΔSCF. *Phys. Chem. Chem. Phys.* **2022**, *24*, 5669–5679.

(34) Behler, J.; Reuter, K.; Scheffler, M. Nonadiabatic effects in the dissociation of oxygen molecules at the Al(111) surface. *Phys. Rev. B Condens. Matter* **2008**, *77*, 115421.

(35) Gilbert, A. T. B.; Besley, N. A.; Gill, P. M. W. Self-Consistent Field Calculations of Excited States Using the Maximum Overlap Method (MOM). *J. Phys. Chem. A* **2008**, *112*, 13164–13171.

(36) Barca, G. M. J.; Gilbert, A. T. B.; Gill, P. M. W. Simple Models for Difficult Electronic Excitations. *J. Chem. Theory Comput.* **2018**, *14*, 1501–1509.

(37) Barca, G. M.; Gilbert, A. T.; Gill, P. M. Communication: Hartree-Fock description of excited states of H2. *J. Chem. Phys.* **2014**, *141*, 111104.

(38) Levi, G.; Pápai, M.; Henriksen, N. E.; Dohn, A. O.; Møller, K. B. Solution Structure and Ultrafast Vibrational Relaxation of the PtPOP Complex Revealed by ΔSCF-QM/MM Direct Dynamics Simulations. *J. Phys. Chem. C* **2018**, *122*, 7100–7119.

(39) Hait, D.; Head-Gordon, M. Excited State Orbital Optimization via Minimizing the Square of the Gradient: General Approach and Application to Singly and Doubly Excited States via Density Functional Theory. *J. Chem. Theory Comput.* **2020**, *16*, 1699–1710.

(40) Kumar, C.; Luber, S. Robust ΔSCF calculations with direct energy functional minimization methods and STEP for molecules and materials. *J. Chem. Phys.* **2022**, *156*, 154104.

(41) Frank, I.; Hutter, J.; Marx, D.; Parrinello, M. Molecular dynamics in low-spin excited states. *J. Chem. Phys.* **1998**, *108*, 4060–4069.

(42) Kowalczyk, T.; Tsuchimochi, T.; Chen, P. T.; Top, L.; Van Voorhis, T. Excitation energies and Stokes shifts from a restricted open-shell Kohn-Sham approach. *J. Chem. Phys.* **2013**, *138*, 164101.

(43) Breit, G. Dirac's equation and the spin-spin interactions of two electrons. *Phys. Rev.* **1932**, *39*, 616–624.

(44) McWeeny, R. *Spins in chemistry*; Dover Publications: Mineola, N.Y, 2004.

(45) Fedorov, D. G.; Gordon, M. S. A study of the relative importance of one and two-electron contributions to spin-orbit coupling. *J. Chem. Phys.* **2000**, *112*, 5611–5623.

(46) Bourne Worster, S.; Feighan, O.; Manby, F. R. Reliable transition properties from excited-state mean-field calculations. *J. Chem. Phys.* **2021**, *154*, 124106.

(47) Löwdin, P.-O. Quantum Theory of Many-Particle Systems. I. Physical Interpretations by Means of Density Matrices, Natural Spin-Orbitals, and Convergence Problems in the Method of Configurational Interaction. *Phys. Rev.* **1955**, *97*, 1474–1489.

(48) Szabo, A.; Ostlund, N. S. *Modern quantum chemistry: introduction to advanced electronic structure theory*; Dover publications, Inc.: New York, 1996.

(49) Tavernelli, I.; Curchod, B. F. E.; Laktionov, A.; Rothlisberger, U. Nonadiabatic coupling vectors for excited states within time-dependent density functional theory in the Tamm–Dancoff approximation and beyond. *J. Chem. Phys.* **2010**, *133*, 194104.

(50) Franco De Carvalho, F.; Curchod, B. F.; Penfold, T. J.; Tavernelli, I. Derivation of spin-orbit couplings in collinear linear-response TDDFT: A rigorous formulation. *J. Chem. Phys.* **2014**, *140*, 144103.

(51) Gao, X.; Bai, S.; Fazzi, D.; Niehaus, T.; Barbatti, M.; Thiel, W. Evaluation of Spin-Orbit Couplings with Linear-Response Time-Dependent Density Functional Methods. *J. Chem. Theory Comput.* **2017**, *13*, 515–524.

(52) Yin, H. M.; Rowling, S. J.; Büll, A.; Kable, S. H. Photodissociation dynamics of the reaction H2 CO→H+HCO via the singlet (S0) and triplet (T1) surfaces. *J. Chem. Phys.* **2007**, *127*, 064302.

(53) Miller, R. G.; Lee, E. K. C. Single vibronic level photochemistry of formaldehydes in the ? 1A2 state: Radiative and nonradiative processes in H2CO, HDCO, and D2CO. *J. Chem. Phys.* **1978**, *68*, 4448–4464.

(54) Yates, B. F.; Yamaguchi, Y.; Schaefer, H. F. The dissociation mechanism of triplet formaldehyde. *J. Chem. Phys.* **1990**, *93*, 8798–8807.

(55) Bowman, J. M.; Zhang, X. New insights on reaction dynamics from formaldehyde photodissociation. *Phys. Chem. Chem. Phys.* **2006**, *8*, 321–332.

(56) Shepler, B. C.; Epifanovsky, E.; Zhang, P.; Bowman, J. M.; Krylov, A. I.; Morokuma, K. Photodissociation dynamics of formaldehyde initiated at the T1/S0 minimum energy crossing configurations. *J. Phys. Chem. A* **2008**, *112*, 13267–13270.

(57) Fu, B.; Shepler, B. C.; Bowman, J. M. Three-state trajectory surface hopping studies of

the photodissociation dynamics of formaldehyde on ab initio potential energy surfaces. *J. Am. Chem. Soc.* **2011**, *133*, 7957–7968.

(58) Jacob, C. R.; Reiher, M. Spin in density-functional theory. *Int. J. Quantum Chem.* **2012**, *112*, 3661–3684.

(59) Macetti, G.; Genoni, A. Initial Maximum Overlap Method for Large Systems by the Quantum Mechanics/Extremely Localized Molecular Orbital Embedding Technique. *J. Chem. Theory Comput.* **2021**, *17*, 4169–4182.

(60) Davidson, E. R.; Clark, A. E. Analysis of wave functions for open-shell molecules. *Phys. Chem. Chem. Phys.* **2007**, *9*, 1881–1894.

(61) Tapavicza, E.; Tavernelli, I.; Rothlisberger, U.; Filippi, C.; Casida, M. E. Mixed time-dependent density-functional theory/classical trajectory surface hopping study of oxirane photochemistry. *J. Chem. Phys.* **2008**, *129*, 124108.

(62) Tavernelli, I.; Curchod, B. F. E.; Rothlisberger, U. On nonadiabatic coupling vectors in time-dependent density functional theory. *J. Chem. Phys.* **2009**, *131*, 196101.

(63) Hu, C.; Sugino, O.; Hirai, H.; Tateyama, Y. Nonadiabatic couplings from the Kohn-Sham derivative matrix: Formulation by time-dependent density-functional theory and evaluation in the pseudopotential framework. *Phys. Rev. A* **2010**, *82*, 062508.

(64) Leticia, G., Lindh, R., Eds. *Quantum Chemistry and Dynamics of Excited States: Methods and Applications*, hardcover ed.; Wiley, 2021.

(65) De Souza, B.; Farias, G.; Neese, F.; Izsák, R. Predicting Phosphorescence Rates of Light Organic Molecules Using Time-Dependent Density Functional Theory and the Path Integral Approach to Dynamics. *J. Chem. Theory Comput.* **2019**, *15*, 1896–1904.

(66) Bussy, A.; Hutter, J. Efficient and low-scaling linear-response time-dependent density

functional theory implementation for core-level spectroscopy of large and periodic systems. *Phys. Chem. Chem. Phys.* **2021**, *23*, 4736–4746.

(67) Hirata, S.; Head-Gordon, M. Time-dependent density functional theory within the Tamm-Dancoff approximation. *Chem. Phys. Lett.* **1999**, *314*, 291–299.

(68) Wang, Z.; Wu, C.; Liu, W. NAC-TDDFT: Time-Dependent Density Functional Theory for Nonadiabatic Couplings. *Acc. Chem. Res.* **2021**, *54*, 3288–3297.

(69) Alary, F.; Boggio-Pasqua, M.; Heully, J. L.; Marsden, C. J.; Vicendo, P. Theoretical characterization of the lowest triplet excited states of the tris-(1,4,5,8-tetraazaphenanthrene) ruthenium dication complex. *Inorg. Chem.* **2008**, *47*, 5259–5266.

(70) Maurer, R. J.; Reuter, K. Assessing computationally efficient isomerization dynamics: ΔSCF density-functional theory study of azobenzene molecular switching. *J. Chem. Phys.* **2011**, *135*, 224303.

(71) Szalay, V. Eckart-Sayvetz conditions revisited. *J. Chem. Phys.* **2014**, *140*.

(72) Franco De Carvalho, F.; Pignedoli, C. A.; Tavernelli, I. TDDFT-Based Spin-Orbit Couplings of 0D, 1D, and 2D Carbon Nanostructures: Static and Dynamical Effects. *J. Phys. Chem. C* **2017**, *121*, 10140–10152.

(73) Granucci, G.; Persico, M.; Spighi, G. Surface hopping trajectory simulations with spin-orbit and dynamical couplings. *J. Chem. Phys.* **2012**, *137*, 22A501.

(74) Tully, J. C. Molecular dynamics with electronic transitions. *J. Chem. Phys.* **1990**, *93*, 1061–1071.

(75) Belyaev, A. K.; Lebedev, O. V. Nonadiabatic nuclear dynamics of atomic collisions based on branching classical trajectories. *Phys. Rev. A* **2011**, *84*, 014701.

(76) Franco de Carvalho, F.; Tavernelli, I. Nonadiabatic dynamics with intersystem crossings: A time-dependent density functional theory implementation. *J. Chem. Phys.* **2015**, *143*, 224105.

(77) Suchan, J.; Janoš, J.; Slavíček, P. Pragmatic Approach to Photodynamics: Mixed Landau-Zener Surface Hopping with Intersystem Crossing. *J. Chem. Theory Comput.* **2020**, *16*, 5809–5820.

(78) Bian, X.; Wu, Y.; Teh, H.-H.; Zhou, Z.; Chen, H.-T.; Subotnik, J. E. Modeling nonadiabatic dynamics with degenerate electronic states, intersystem crossing, and spin separation: A key goal for chemical physics. *J. Chem. Phys.* **2021**, *154*, 110901.

(79) Wu, Y.; Subotnik, J. E. Semiclassical description of nuclear dynamics moving through complex-valued single avoided crossings of two electronic states. *J. Chem. Phys.* **2021**, *154*, 234101.

(80) Hammes-Schiffer, S.; Tully, J. C. Proton transfer in solution: Molecular dynamics with quantum transitions. *J. Chem. Phys.* **1994**, *101*, 4657–4667.

(81) Brillouin, L. Les problèmes de perturbations et les champs self-consistents. *J. Phys. Radium* **1932**, *3*, 373–389.

(82) Brillouin, L. Le champ self-consistent de Fock pour les électrons des métaux. *J. Phys. Radium* **1934**, *5*, 413–418.

(83) Akimov, A. V. Nonadiabatic Molecular Dynamics with Tight-Binding Fragment Molecular Orbitals. *J. Chem. Theory Comput.* **2016**, *12*, 5719–5736.

(84) Helgaker, T.; Jorgensen, P.; Olsen, J. *Molecular electronic-structure theory*; John Wiley & Sons: Chichester, England, 2000.

(85) Koch, W.; Holthausen, M. C. *A Chemist's Guide to Density Functional Theory*; Wiley, 2001.

(86) Engel, E.; Dreizler, R. M. *Density Functional Theory - An Advanced Course*; Springer Berlin Heidelberg, 2011.

(87) Zhang, Y.; Yang, W. A challenge for density functionals: Self-interaction error increases for systems with a noninteger number of electrons. *J. Chem. Phys.* **1998**, *109*, 2604–2608.

(88) CP2K Program Package, CP2K Developers Group, Version 8.0, https://www.cp2k.org/. Accessed on 08.04.2022.

(89) Adamo, C.; Barone, V. Toward reliable density functional methods without adjustable parameters: The PBE0 model. *J. Chem. Phys.* **1999**, *110*, 6158–6170.

(90) Guidon, M.; Hutter, J.; VandeVondele, J. Auxiliary Density Matrix Methods for Hartree-Fock Exchange Calculations. *J. Chem. Theory Comput.* **2010**, *6*, 2348–2364.

(91) Weigend, F.; Ahlrichs, R. Balanced basis sets of split valence, triple zeta valence and quadruple zeta valence quality for H to Rn: Design and assessment of accuracy. *Phys. Chem. Chem. Phys.* **2005**, *7*, 3297–3305.

(92) VandeVondele, J.; Hutter, J. Gaussian basis sets for accurate calculations on molecular systems in gas and condensed phases. *J. Chem. Phys.* **2007**, *127*, 114105.

(93) Goedecker, S.; Teter, M.; Hutter, J. Separable dual-space Gaussian pseudopotentials. *Phys. Rev. B* **1996**, *54*, 1703–1710.

(94) Perdew, J. P.; Burke, K.; Ernzerhof, M. Generalized Gradient Approximation Made Simple. *Phys. Rev. Lett.* **1996**, *77*, 3865–3868.

(95) Perdew, J. P.; Burke, K.; Ernzerhof, M. Generalized gradient approximation made simple (vol 77, pg 3865, 1996). *Phys. Rev. Lett.* **1997**, *78*, 1396–1396.

(96) Ditchfield, R.; Hehre, W. J.; Pople, J. A. Self-consistent molecular-orbital methods. IX. An extended gaussian-type basis for molecular-orbital studies of organic molecules. *J. Chem. Phys.* **1971**, *54*, 720–723.

(97) Hehre, W. J.; Ditchfield, K.; Pople, J. A. Self-consistent molecular orbital methods. XII. Further extensions of gaussian-type basis sets for use in molecular orbital studies of organic molecules. *J. Chem. Phys.* **1972**, *56*, 2257–2261.

(98) Hariharan, P. C.; Pople, J. A. The influence of polarization functions on molecular orbital hydrogenation energies. *Theor. Chim. Acta* **1973**, *28*, 213–222.

(99) Zagreb surface hopping code, 2018; available from `https://e-cam.readthedocs.io/en/latest/Quantum-Dynamics-Modules/modules/zagreb_sh/z` . Accessed on 08.04.2022.

(100) Mališ, M.; Agostini, F.; Sanz-Sanz, C.; Ehrmaier, J.; MacKernan, D.; Lauvergnat, D.; Bonella, S. D3.4.: Quantum Dynamics E-CAM modules III. **2018**,

(101) Sapunar, M.; Piteša, T.; Davidović, D.; Došlić, N. Highly Efficient Algorithms for CIS Type Excited State Wave Function Overlaps. *J. Chem. Theory Comput.* **2019**, *15*, 3461–3469.

(102) Neese, F. The ORCA program system. *Wiley Interdiscip. Rev. Comput. Mol. Sci.* **2012**, *2*, 73–78.

(103) Neese, F. Software update: the ORCA program system, version 4.0. *Wiley Interdiscip. Rev. Comput. Mol. Sci.* **2018**, *8*, 1327.

TOC Graphic